Optics & Laser Technology 168 (2024) 109937

Contents lists available at ScienceDirect

Optics and Laser Technology

journal homepage: www.elsevier.com/locate/optlastec

Full length article

Ultrashort pulsed beam induced nanoparticles displacement trajectories via optical forces in symmetrical and symmetry-breaking systems

Maya Hen Shor Peled [a], Fyodor Morozko [a], Andrey Novitsky [b], Paolo Maioli [c], Alina Karabchevsky [a,*]

[a] School of Electrical and Computer Engineering, Ben-Gurion University of the Negev, Beer-Sheva, 8410501, Israel
[b] Department of Physical Optics and Applied Informatics, Belarusian State University, Belarus
[c] Institut Lumière Matière (ILM), CNRS and Université de Lyon, Villeurbanne, France

ARTICLE INFO

Keywords:
Nanoparticles
Ultrashort pulses
Optical manipulation
Optical force
Attractive or repulsive forces
Photonic jet
Photonic hook

ABSTRACT

Optical manipulation provides new insight into a wide range of physical phenomena and has engendered advanced applications in various fields. By utilizing near-field methods that overcome the diffraction limit, the ability to manipulate nanoparticles became feasible. In this paper, we analyze the displacement trajectories of a gold nanoparticle in the field of an ultrashort pulsed beam in symmetric (photonic nanojet) and symmetry-breaking (photonic hook) systems. We generate a symmetric optical force by illuminating a dielectric, micro-cylinder, and break the symmetry by adding a dielectric plate. We developed an efficient numerical method for calculating nanoparticle displacement under pulsed illumination which uses a stroboscopic map. Within this method, we revealed the influence of the plate position on the likeliness of different types of nanoparticle motion (i.e. stable, negative, or positive motion) in symmetric and symmetry-breaking configurations. Our work stimulates the development of experimental methods for optomechanical manipulation and opens a venue for future fundamental investigations for a range of practical applications, where accurate control over the mechanical motion of nanoscale objects is required.

1. Introduction

Over the past few decades, optical trapping and manipulation of particles, driven by the ability to tailor light through spatial control of its amplitude, phase, and polarization, has attracted significant interest from researchers [1]. Ashkin's pioneering work on optical tweezers has promoted significant advances in cellular and molecular biology through the ability to trap and detect small objects [2]. However, optical tweezers are insufficient when applied for the manipulation of nano-objects such as Rayleigh particles and bio-molecules, due to the fundamental diffraction limit of light [3]. By attaching bio-molecules to dielectric micro-beads, optical tweezers can be used to trap the beads, which are used as handles for manipulating the molecules in biomechanical studies [4,5]. Yet, direct manipulation of particles with nanoscale dimensions based on light–matter interactions is not possible with optical tweezers. Achieving manipulation on the nanoscale level requires auxiliary structures that generate tightly confined electric fields. Near-field methods such as plasmonic tweezers [6–9] and photonic crystal resonators [10] overcome the diffraction limitation, yet excessive heating could be destructive to the biological environment due to the accumulated heat effect induced by continuous wave (CW) illumination. Pulsed illumination can be employed for reducing heating effects, the time between pulses allows for the nanoparticle to cool down, a process which, in the case of metallic nanoparticles, is in the order of tens to hundreds of picoseconds [11–13]. For equivalent total energy injected into the system, the time and position-dependent thermal patterns are very different in the case of pulsed illumination, which makes this method non-destructive in situations for which CW illumination can be detrimental. Optical manipulation with pulsed illumination has been explored in various studies as a tool for reducing the damage of living samples [14–16], and for increasing trapping stability of particles in the Rayleigh regime [17]. To confine light into a narrow spot, symmetric systems generating photonic nano-jets (PNJ) were proposed [18]. PNJs are high-intensity, sub-wavelength light beams generated by dielectric structures that are subjected to illumination by a plane wave [19]. Such symmetric systems generating a narrow beam have found applications in numerous fields such as super-resolution microscopy [18,20], nano-patterning [21], and signal enhancing for different characterization techniques [18,22,23]. Due to the strong optical confinement of the PNJ, it provides new possibilities for the optical manipulation of nanoparticles. Previous studies have

* Corresponding author.
E-mail addresses: shormaya@post.bgu.ac.il (M.H.S. Peled), alinak@bgu.ac.il (A. Karabchevsky).

https://doi.org/10.1016/j.optlastec.2023.109937
Received 11 June 2023; Received in revised form 16 July 2023; Accepted 7 August 2023
Available online 22 August 2023
0030-3992/© 2023 Elsevier Ltd. All rights reserved.

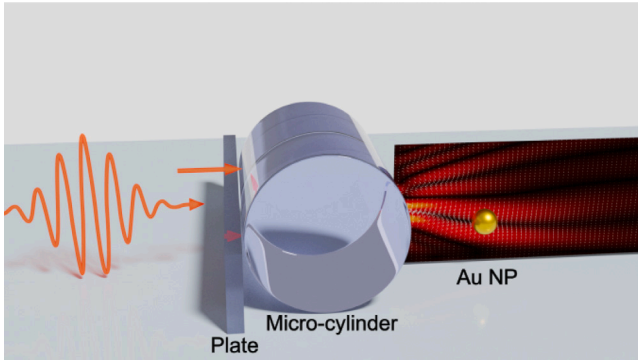

Fig. 1. Artistic illustration of the studied system. A pulsed beam illuminates a dielectric micro-cylinder. The symmetry or symmetry-breaking properties of the system are induced by a dielectric plate, to create an optical force exerted on a gold nanoparticle.

experimentally demonstrated the trapping of nanoparticles using PNJs generated by CW illumination [3,24–26], and the optical forces exerted on them [27]. When the symmetry of a system generating PNJ is broken, either by an asymmetrical geometry of an auxiliary structure [13,28–31], asymmetrical optical properties [32] or asymmetrical illumination [33,34], the generated light beam becomes curved. This effect is known as a photonic hook (PH), its curvature is obtained by the difference between the phase velocity and the interference of the waves inside the auxiliary structure [35]. The PH is a curved, high-intensity focused beam that has the attractive properties of optical confinement, similar to the PNJ, and can be utilized for nanoparticle manipulation in a curved trajectory. PH-based optical manipulation was previously explored under continuous and pulsed illumination for an asymmetric auxiliary structure [13], yet the construction of such a structure requires complicated fabrication processes. Furthermore, the effect of pulsed illumination on the nanoparticle was investigated only for a single pulse. To compare the realistic effect of pulsed illumination, it is necessary to compute the effect on a longer timescale which takes into account the nanoparticle displacement and velocity between a cascade of subsequent pulses.

Here, we report on the investigation of the optical forces exerted on a 30 nm radius gold nanoparticle, generated in symmetric and symmetry-breaking configurations. In the symmetric configuration, the beam with the wavelength $\lambda_0 = 500$ nm illuminates a dielectric micro-cylinder of 1 μm radius, to produce a PNJ. In contrast, the symmetry-breaking configuration occurs when the plate (of the same material) is placed before the cylinder, the field becomes a PH. Fig. 1 shows an artistic illustration of the setup able to generate the requested optical fields. We investigate different symmetry-breaking configurations, meaning different plate heights, and simulate the nanoparticle motion induced by each configuration. We efficiently calculate the nanoparticle displacement under pulsed illumination using a stroboscopic map. We study how nanoparticle's initial position changes its motion, and which type of motion (stable, positive, or negative direction) are more probable with each configuration. The outcomes of our research are essential for designing experimental systems for the optical manipulation of nanoparticles. By controlling plate position, one may change the optical field and affect the nanoparticle motion. This, in turn, can be applied in medical therapy, diagnosis and drug delivery, to name a few.

2. Methods

We study the effect of illuminating with pulsed and CW light at 500 nm wavelength. The electric fields are simulated using Ansys Lumerical FDTD with Perfectly Matched Layer (PML) boundary conditions. The scattered field formalism is used with an initial plane wave propagating along the x-axis, and the electric field polarized along the y-axis. The dielectric micro-cylinder is chosen to have a 1 μm radius and refractive index of 1.4, corresponding to PDMS due to the simplicity of fabrication method [36]. The plate is chosen to have a 0.5 μm width and 1.5 μm length, with the same refractive index. Six different configurations of cylinder and plate were studied: (1) with no plate; with the plate being positioned at the height of (2) an eighth; (3) a quarter; (4) a third; (5) half; and at (6) three quarters of the cylinder diameter. The whole system is studied in air. We used an unchirped Gaussian pulse of 100 fs duration in terms of FWHM, which corresponds to a bandwidth of 4.4 THz at 500 nm central wavelength. The mesh is refined along x and y axes to have a size of 0.01 μm with a field-time monitor. The incident field amplitude is chosen to be 6000 V/m and 2 MV/m for CW and pulsed illumination respectively, corresponding to the same average power and to realistic conditions.

Our goal is to reveal the dynamics of gold nanoparticles. The optical forces acting on nanoparticles can be calculated within the electric dipole approximation [37], since the radius of the nanoparticle ($R = 30$ nm) is much smaller than the incident wavelength ($\lambda_0 = 500$ nm). At this wavelength, the imaginary part of the polarizability is highest, which is directly related to the optical force [13]. The optical force reads as

$$\vec{F} = (\vec{p}\cdot\nabla)\vec{E} + \dot{\vec{p}}\times\vec{B}, \tag{1}$$

where $\vec{p}$ is the electric dipole moment, dot is the time derivative and $\vec{E}$ and $\vec{B}$ are the electric and magnetic fields, respectively. In general, the field time-dependence includes rapid oscillations at the carrier frequency $\omega_0 = 2\pi c/\lambda_0$ (c is the speed of light in vacuum) and slow modulation. After the cycle-averaging we arrive at the optical force

$$\langle\vec{F}\rangle = \sum_i \frac{1}{2}\mathrm{Re}\{p_i^*\nabla E_i\}. \tag{2}$$

where the asterisk * stands for the complex conjugation. The force $\langle\vec{F}\rangle$ may slowly depend on time and the dependence can be treated as parametric. By writing the dipole moment as

$$\vec{p}(t) = \alpha(\omega_0)\vec{E}(t) \tag{3}$$

and polarizability of the metallic nanoparticle as $\alpha = \alpha' + i\alpha''$, we obtain

$$\langle\vec{F}\rangle = \frac{\alpha'}{2}\sum_i \mathrm{Re}\{E_i^*\nabla E_i\} + \frac{\alpha''}{2}\sum_i \mathrm{Im}\{E_i^*\nabla E_i\}. \tag{4}$$

Note that in Eq. (3) we neglect the dispersion of the polarizability. Although in general dispersion must be accounted for in the case of pulsed light, the light spectrum in the femtosecond pulse regime is narrow enough for the polarizability to remain approximately constant.

If the field can be presented as a product of rapidly varying phase factor and slow function of coordinates, $\vec{E} = \vec{E}_0(\vec{r})\exp(i\vec{k}\cdot\vec{r})$, then the first term of Eq. (4) describes the gradient force, $\vec{F}_{\mathrm{grad}} = \frac{\alpha'}{4}\nabla|\vec{E}_0|^2$, proportional to the real part (dispersive part) of the complex polarizability. This force is responsible for accelerating the particle towards the field intensity gradient and therefore can be used to trap a particle in a tightly focused laser beam at its focus. The second term of Eq. (4) is known as the scattering force, $\vec{F}_{\mathrm{scat}} = \frac{\alpha''}{2}|\vec{E}_0|^2\vec{k}$, proportional to the imaginary part (dissipative part) of the complex polarizability. This force is a consequence of the momentum exchange from the field to the particle. The scattering force pushes the absorbing particle in the direction of propagation and can result in the particle escaping the trap if the focusing is not tight enough [37].

Complex polarizability of the electric dipole generally includes the radiation (Draine) correction as

$$\alpha = \frac{\alpha_0}{1 - ik_0^3\alpha_0/6\pi\epsilon_0}, \tag{5}$$

where the static polarizability α_0 can be written using the Clausius–Mossotti relation for spherical nanoparticles [38,39]:

$$\alpha_0 = 4\pi R^3\epsilon_0\frac{\epsilon_p - \epsilon_m}{\epsilon_p + 2\epsilon_m}. \tag{6}$$

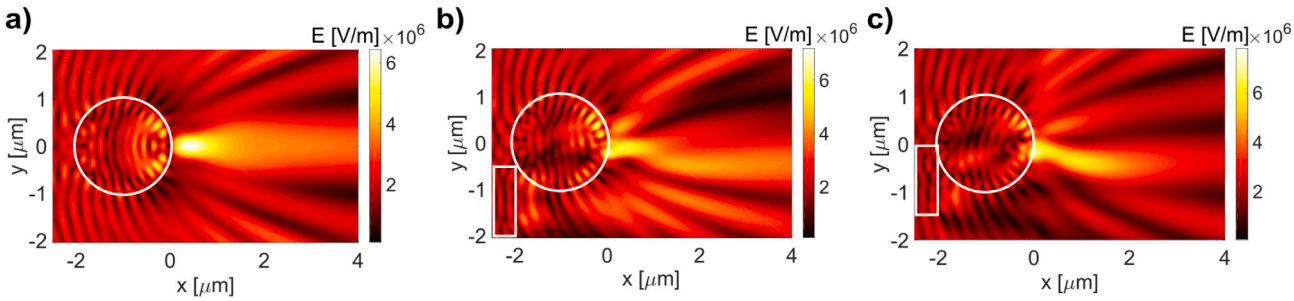

Fig. 2. Calculated electric field generated by pulsed illumination. We study three configurations: (a) a symmetrical system generating PNJ; (b) a system with broken symmetry in which a plate is positioned at a quarter of the cylinder diameter; and (c) when a plate is positioned at half of the cylinder diameter.

Here $k_0 = 2\pi/\lambda_0$ and ϵ_p, ϵ_m and ϵ_0 are the dielectric constants of the nanoparticle, surrounding medium and free space, respectively. The dielectric constant of the gold nanoparticle was obtained by fitting the experimental data of Johnson and Christy [40] to calculations of the real and imaginary dielectric function, which include Drude and interband contributions at room temperature [12]. The small nanoparticles, as in our case, can be well described by the static polarizability $\alpha \approx \alpha_0$.

Motion of a particle in a time-dependent field of force $\vec{F}(\vec{r},t)$ is governed by the Newton's equations of motion

$$\dot{\vec{v}} = \frac{1}{m}\vec{F}(\vec{r},t),\ \dot{\vec{r}} = v, \tag{7}$$

where $\vec{r}$ and $\vec{v}$ are the position and velocity of the particle, respectively, m is the particle's mass. In general, these equations cannot be solved in quadratures since the force distribution is a nontrivial function of the coordinates. The equation can be rather solved numerically e.g., using Euler or Runge–Kutta method. For a nanoparticle in a pulsed illumination field, it is, however, possible to obtain the solution for the equation in quadratures. In order to do this we observe that (1) between the pulses the nanoparticle moves uniformly (in the absence of friction) and that (2) the position of the nanoparticle almost does not change within the duration of one pulse. This allows us to integrate the equations of motion in quadratures. As a result, we obtain a stroboscopic motion of the nanoparticle in the field of the pulse train:

$$\vec{v}_{n+1} = \vec{v}_n + \frac{1}{m}\Delta\vec{P}(\vec{r}_n),\ \vec{r}_{n+1} = \vec{r}_n + \vec{v}_{n+1}T, \tag{8}$$

where $\Delta\vec{P}(\vec{r}) = \int_0^\tau \vec{F}(\vec{r},t)dt$ is the added momentum transmitted by light, $T = t_{n+1} - t_n$ is the time between pulses, τ is the duration of the pulse. In the second part of Eq. (8) we have used the fact that the duration of the pulse is much shorter than the time between the pulses $\tau \ll T$ so that $T - \tau \approx T$.

In summary, the procedure of calculating a nanoparticle's motion is as follows: (1) Obtain the electric and magnetic fields $\vec{E}(\vec{r},t)$, $\vec{H}(\vec{r},t)$ for the time during a single pulse $[0,\tau]$ for a given geometry using Finite-Difference Time-Domain (FDTD) simulations; (2) Calculate force $\vec{F}(\vec{r},t)$ from fields using Eqs. (1), (3), (5) and (6); (3) Calculate the added momentum $\Delta\vec{P}(\vec{r})$ by numerically integrating the force field $\vec{F}(\vec{r},t)$ over the FDTD simulation time interval $[0,\tau]$; (4) Calculate nanoparticle's trajectories for different initial positions using the calculated $\Delta\vec{P}(\vec{r})$.

The procedure requires only a single FDTD simulation per scattering geometry. Furthermore, calculating nanoparticle's motion using the stroboscopic map (8) reduces simulation time by several orders of magnitude as compared to the numerical integration of Eq. (7) while producing indistinguishable trajectories.

3. Results and discussion

Fig. 2 demonstrates the comparison between the spatial electric field distributions of optical forces generated in symmetric and symmetry-broken systems for two plate positions, under pulsed illumination. Due to plate positioning before the cylinder, the phase of the transmitted wave evolves, thus providing the PH configuration. The electric field becomes asymmetric, illustrating a curved deformation that forms the PH near the shadow side of the cylinder. Note that the plate here is of the same material as the cylinder.

To compare the effect of pulsed illumination with continuous wave (CW) illumination, in the former case we apply 100 fs pulses every 10 ns. Heating of the nanoparticle does not affect its motion either during the short time (100 fs) of application of the force field or at the next pulse time moment because the particle has time to cool down between pulses [11]. More specifically, the thermal-induced, nonlinear metal dielectric function (ϵ_p) variations during ultrashort excitation are negligible [12], and at the same time, no thermophoretic forces apply as the nanoparticle temperature is always spatially homogeneous. The pulse parameters chosen are typica of Ti:Sapphire lasers. One could choose a different repetition time, as long as it is larger than a few picoseconds, which is the time it takes for the nanoparticle to cool.

Figs. 3, 4, and 5 show optical forces applied on the gold nanoparticle for three different configurations under pulsed illumination: cylinder with no plate to create a PNJ, cylinder with a plate positioned at a quarter of its height, and cylinder with a plate positioned at half of its height, both creating a PH. The insets show different types of nanoparticle trajectories, starting from initial positions corresponding to the blue dots. The nanoparticle is illuminated for 20 ms (corresponding to 2×10^6 pulses) for all cases under the study. As the instantaneous power of pulsed illumination is chosen for obtaining the same average power as that in CW conditions, the optical forces of pulsed illumination are five orders of magnitude higher both for PNJ and PH according to 10 ns/100 fs ratio. We note, that under CW illumination, the nanoparticle experiences a negligible displacement of about a few picometers. We explain this minor displacement by the insufficient time duration set as 20 ms. We hypothesize that if the illumination time is longer the displacement would be larger. On the other hand, under pulsed illumination, for the same duration of 20 ms, the nanoparticle exhibits a much larger displacement.

When simulating the nanoparticle motion for all three cases, we noticed three types of motion: negative direction motion, where the nanoparticle is being attracted towards the cylinder (coordinate x decreases); positive direction motion, where the nanoparticle is being repulsed (coordinate x increases); and an oscillatory motion, where the nanoparticle is confined within a finite region (around or between stable points). It should be noted that the input pulse intensity does not change the amplitude of the oscillating motion. This means that the motion is produced by a great number of pulses. In addition, only after a sufficient number of pulses (around 100k pulses) does the nanoparticle's displacement take place in all of the cases. This can be explained by the accumulated effect of absorbing enough energy for initiating motion (for a sufficient increase of particle's velocity). Increasing pulse intensity would result in an earlier initiation of the nanoparticle's displacement. Other pulse parameters, such as wavelength, would induce a different optical force since at the chosen wavelength the imaginary part of the polarizability is highest [13], which is proportional to the

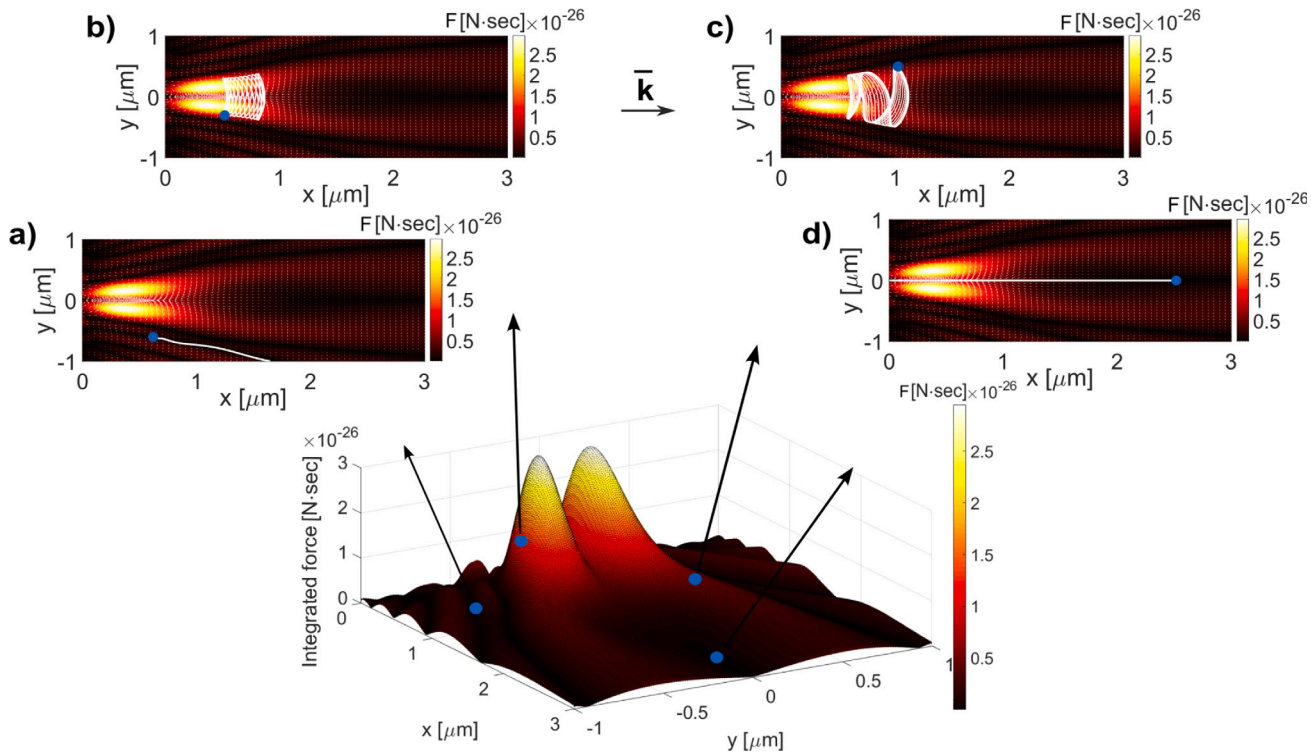

Fig. 3. Optical force as a function of particle position for the symmetric system case generating PNJ under pulsed illumination. The insets show the nanoparticle trajectory corresponding to the initial position marked by a blue dot, where (a) (0.6,−0.6); (b) (0.5,−0.3); (c) (1,0.5); and (d) (2.5,0). The direction of vector k is indicated by the arrow placed in the middle between subplot b and subplot c.

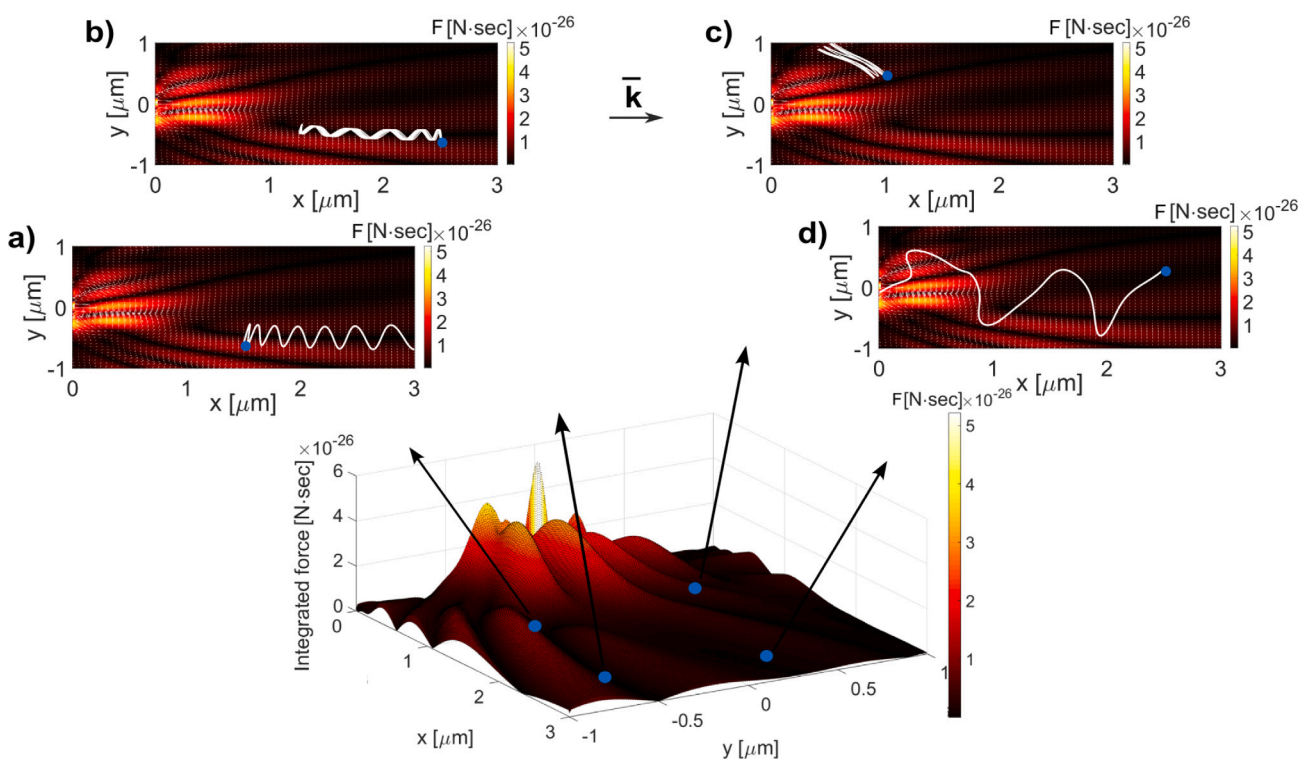

Fig. 4. Optical force as a function of particle position when the plate is positioned at a quarter of cylinder diameter generating a PH under pulsed illumination. The insets show the nanoparticle trajectory corresponding to the initial position marked by a blue dot where (a) (1.5,−0.6); (b) (2.5,−0.6); (c) (1,0.5); and (d) (2.5,0.3). The direction of vector k is indicated by the arrow placed in the middle between subplot b and subplot c.

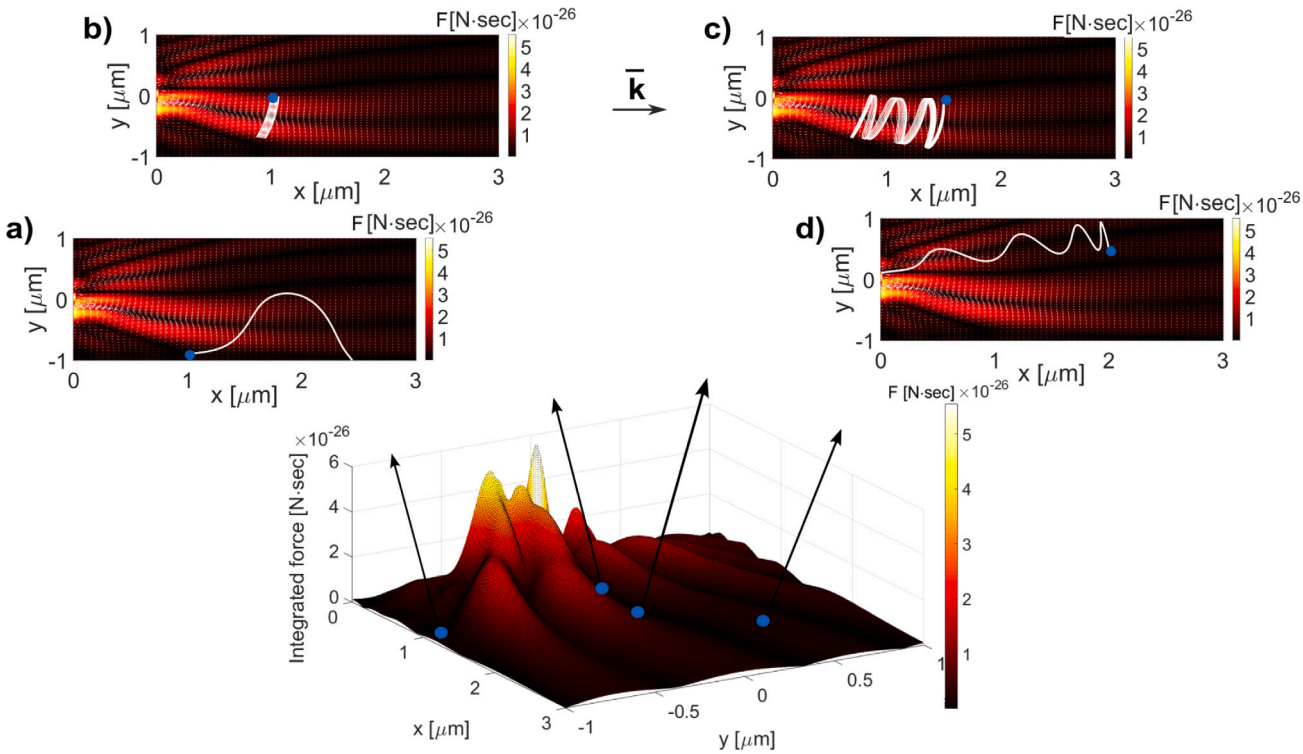

Fig. 5. Optical force as a function of particle position where the plate is placed at half of the cylinder diameter generating a PH under pulsed illumination. The insets show the nanoparticle trajectory corresponding to the initial position marked by a blue dot where (a) (1,−0.9); (b) (1,0); (c) (1.5,0); and (d) (2,0.5). The direction of vector k is indicated by the arrow placed in the middle between subplot b and subplot c.

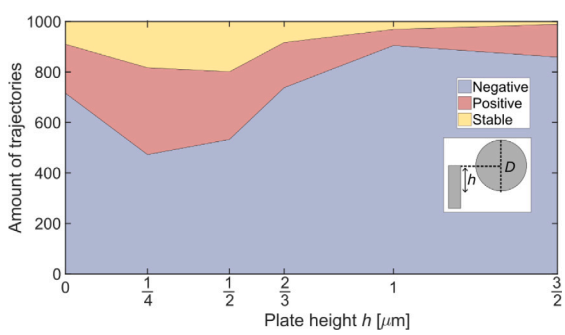

Fig. 6. Area plot showing the number of each type of motion depending on symmetry/symmetry-breaking properties of the system. Symmetry is broken by positioning the plate at 6 different heights (noted by h, described in inset). Note: 1000 trajectories were simulated for each configuration.

scattering force (as seen in Eq. (4)). This would eventually result in a different type of nanoparticle motion.

Fig. 3 shows an optical force map of the PNJ, which field is symmetric with respect to the y axis. In the insets, we show the three types of motion introduced above. The most common type of motion is the negative direction motion of the nanoparticle towards the cylinder as in Fig. 3d. When placing the nanoparticle at the point (0.6,−0.6) μm (Fig. 3a), the nanoparticle moves in the positive direction, outwards from the cylinder. If the nanoparticle was shifted 100 nm to the left, then it would move in the negative direction, towards the cylinder. These different types of motion are highly dependent on the initial position, and a slight change in direction might change the motion. There are also stable points in the force map. When positioning the nanoparticle in their vicinity, it makes a finite motion oscillating around the stable point. Figs. 3b and c showcase two positions leading to different types of finite oscillations. In Fig. 3b, the nanoparticle oscillates with an amplitude of between 600 − 800 nm and is symmetric with respect to the axis $y = 0$, whereas in Fig. 3c the amplitude is 1 μm and the finite oscillatory motion of the nanoparticle is asymmetric. Due to the symmetry of the PNJ field around the line $y = 0$, the types of motion are the same for the initial positions of the nanoparticles at points (x, y) and $(x, -y)$.

Fig. 4 demonstrates the optical force map when a plate is placed at the height of a quarter of the cylinder diameter. In this configuration, the positive direction motion, where the nanoparticle moves outwards from the cylinder, is more common than in the previous configuration. This motion is shown in Fig. 4a, where the nanoparticle shifts in the oscillatory fashion towards the edge of the simulation area with a 400 nm amplitude. Placed 1 μm to the right, the nanoparticle is trapped and oscillates between two points, corresponding to Fig. 4b. Another initial position that leads to the nanoparticle being trapped is (1,0.5) μm (see Fig. 4c). In this case, the nanoparticle makes 500 nm-amplitude oscillations, being more tightly bounded to the stable point than in Fig. 4b, where the nanoparticle travels back and forth with an almost 1.5 μm amplitude. This configuration of cylinder and plate produces the highest number of stable nanoparticle motions out of the configurations in question. The most common type of movement is negative direction motion, demonstrated in Fig. 4d, where the nanoparticle is attracted towards the cylinder. This shows that the attraction of the nanoparticle by an electromagnetic wave is not only for particles placed near intensity maximum (due to the gradient force) or is related to field symmetry (like in the case of PNJ), but can be realized for particles placed at longer distances in asymmetric fields.

Fig. 5 shows the optical force map when the plate is placed at the height of half of the cylinder diameter. Out of the three available configurations, this one produces the highest number of negative direction motions, one of which is shown in Fig. 5d, where the nanoparticle is attracted towards the cylinder at axis $y = 0$. If the nanoparticle is placed at (1,0) μm (Fig. 5b), then it makes an oscillatory motion of 700 nm amplitude, tightly traveling back and forth around a stable point. However, when the initial position of the nanoparticle is displaced 500 nm

to the right (Fig. 5c), the nanoparticle is trapped and oscillates more "loosely", moving almost 1 μm back and forth, with 700 nm amplitude. When placed at position (1, −0.9) μm (Fig. 5a), the nanoparticle moves in the positive direction outwards from the cylinder. However, when placed 200 nm to the left, the nanoparticle is attracted towards the cylinder. These examples show how strongly the trajectory depends on the initial position.

Upon studying these three cylinder and plate configurations, we were curious to find a trend between plate position and type of motion. We added 3 more plate positions ($1/8, 1/3$ and $3/4$) and simulated 1000 trajectories corresponding to 1000 different initial positions. The outcomes of this study are summarized in Fig. 6. We notice that there is a range of plate positions that may induce a higher probability of each type of motion. This could be used for designing an experimental approach for manipulating nanoparticles according to the aimed application. For example, as seen in Fig. 6, when the plate is positioned at the height of a quarter of cylinder diameter, it produces the highest number of stable trajectories, where the nanoparticle oscillates around a stable point. This can be applied for medical treatment where focused, mechanical destruction of tissue or matter is needed. Although the type of motion strongly depends on the initial position of the nanoparticle, the particle's location is relative to the incident illumination. To control the particle motion as planned, one can tune the position of the laser respectively. When the plate is positioned at an eighth of the cylinder diameter, this configuration results in the largest number of positive motion directions, outwards from the cylinder. This can be utilized for drug delivery applications in a non-invasive regime, super-resolution imaging by modifying the nanoparticle with a fluorescent molecule, three-dimensional printing, or driving a nanoparticle through a barrier where mechanical force is needed. When the plate is at half of the cylinder diameter, this configuration produces the largest number of negative motion directions, meaning attracting the nanoparticle towards the cylinder. This can be used for removing particles from an environment or sample [38]. For these applications, the extension of PNJ and PH effects in a liquid environment and heating of the latter for CW and pulsed illumination needs to be considered. Although this study was performed on gold nanoparticles, the applications can be directly extended to different metal nanoparticles, since the response of nanoparticles made of other metals is very similar to the one of gold. The illumination parameters would need to be tailored for the specific material and geometry in study, in terms of which wavelength would result in highest optical absorption [41]. In addition, the polarizability would change depending on the different material and shape, and computations must be repeated for the specific geometry and material. To get the precise trend of how the type of motion is related to plate position, more plate positions should be studied. If one wanted to generalize this study in terms of cylinder and plate properties, it should be noted that this trend would differ for different cylinder properties. Particularly, by changing the cylinder diameter, the optical field properties such as full width at half maximum, focal distance, and maximal intensity change, along with the tilt angle in the symmetry-breaking case [34]. This would, in turn, induce a different nanoparticle behavior and trend in terms of plate position. In addition, changing the plate thickness would result in a larger accumulated phase that would change the curvature of the asymmetrical field.

4. Conclusions

To conclude, we have explored the prospects of nanoparticle manipulation under pulsed illumination. We have studied the optical forces exerted on a gold Rayleigh nanoparticle in symmetric and symmetry-breaking systems. We generated an efficient way of calculating the particle displacement under a train of pulses using a stroboscopic map. We have studied different dynamics of the nanoparticle motion and revealed the role of starting position and plate height to affect the type of trajectory. We characterized three types of motion: negative direction motion, where the nanoparticle is being attracted towards the cylinder; positive direction motion, where the nanoparticle is being repulsed outwards; and oscillatory motion, where the nanoparticle oscillates around or between stable points. We have revealed that there is a range of plate positions that may induce a higher probability of each type of motion, which can be utilized for designing an experimental approach for nanoparticle manipulation according to aimed application. Our results are expected to stimulate the development of experimental methods for the optomechanical manipulation of nanoparticles. Optomechanical manipulation opens a venue for future fundamental investigations and a range of practical applications, where accurate control over the mechanical motion of small objects is required, such as drug delivery, super-resolution imaging in low contrast media, thermo-mechanical medical treatment and three-dimensional printing to list a few applications.

CRediT authorship contribution statement

Maya Hen Shor Peled: Investigation, Visualization, Methodology. **Fyodor Morozko:** Investigation, Resources. **Andrey Novitsky:** Investigation, Resources. **Paolo Maioli:** Investigation, Supervision. **Alina Karabchevsky:** Investigation, Supervision, Conceptualization, Resources.

Declaration of competing interest

The authors declare the following financial interests/personal relationships which may be considered as potential competing interests: Alina Karabchevsky reports financial support was provided by Israel Science Foundation.

Data availability

Data will be made available on request.

Acknowledgments

The research was funded by Israel Science Foundation ISF no. 2598/20.

References

[1] A. Karabchevsky, T. Elbaz, A. Katiyi, O. Prager, A. Friedman, Super-resolution imaging and optomechanical manipulation using optical nanojet for nondestructive single-cell research, Adv. Photonics Res. 3 (2) (2022) 2100233.
[2] A. Ashkin, J.M. Dziedzic, T. Yamane, Optical trapping and manipulation of single cells using infrared laser beams, Nature 330 (6150) (1987) 769–771.
[3] Y.-C. Li, H.-B. Xin, H.-X. Lei, L.-L. Liu, Y.-Z. Li, Y. Zhang, B.-J. Li, Manipulation and detection of single nanoparticles and biomolecules by a photonic nanojet, Light Sci. Appl. 5 (12) (2016) e16176.
[4] J. Ma, L. Bai, M.D. Wang, Transcription under torsion, Science 340 (6140) (2013) 1580–1583.
[5] F.M. Fazal, S.M. Block, Optical tweezers study life under tension, Nat. Photonics 5 (6) (2011) 318–321.
[6] J. Berthelot, S.S. Aćimović, M.L. Juan, M.P. Kreuzer, J. Renger, R. Quidant, Three-dimensional manipulation with scanning near-field optical nanotweezers, Nature Nanotechnol. 9 (4) (2014) 295–299.
[7] A. Kotnala, R. Gordon, Quantification of high-efficiency trapping of nanoparticles in a double nanohole optical tweezer, Nano Lett. 14 (2) (2014) 853–856.
[8] M.L. Juan, M. Righini, R. Quidant, Plasmon nano-optical tweezers, Nat. Photonics 5 (6) (2011) 349–356.
[9] A. Grigorenko, N. Roberts, M. Dickinson, Y. Zhang, Nanometric optical tweezers based on nanostructured substrates, Nat. Photonics 2 (6) (2008) 365–370.
[10] Y.-F. Chen, X. Serey, R. Sarkar, P. Chen, D. Erickson, Controlled photonic manipulation of proteins and other nanomaterials, Nano Lett. 12 (3) (2012) 1633–1637.
[11] M. Gandolfi, A. Crut, F. Medeghini, T. Stoll, P. Maioli, F. Vallée, F. Banfi, N. Del Fatti, Ultrafast thermo-optical dynamics of plasmonic nanoparticles, J. Phys. Chem. C 122 (15) (2018) 8655–8666.
[12] T. Stoll, P. Maioli, A. Crut, N. Del Fatti, F. Vallée, Advances in femto-nano-optics: ultrafast nonlinearity of metal nanoparticles, Eur. Phys. J. B 87 (2014) 1–19.

[13] M. Spector, A.S. Ang, O.V. Minin, I.V. Minin, A. Karabchevsky, Temperature mediated 'photonic hook'nanoparticle manipulator with pulsed illumination, Nanoscale Adv. 2 (6) (2020) 2595–2601.
[14] D. Choudhary, A. Mossa, M. Jadhav, C. Cecconi, Bio-molecular applications of recent developments in optical tweezers, Biomolecules 9 (1) (2019) 23.
[15] Y. Hosokawa, R. Yasukuni, S. Yamada, T. Sugiura, Cell manipulations by optical tweezers and laser ablation, in: Handbook of Laser Micro-and Nano-Engineering, Springer, 2020, pp. 1–27.
[16] A. Blázquez-Castro, Optical tweezers: Phototoxicity and thermal stress in cells and biomolecules, Micromachines 10 (8) (2019) 507.
[17] A. Usman, W.-Y. Chiang, H. Masuhara, Optical trapping of nanoparticles by ultrashort laser pulses, Sci. Prog. 96 (1) (2013) 1–18.
[18] Z. Chen, A. Taflove, V. Backman, Photonic nanojet enhancement of backscattering of light by nanoparticles: a potential novel visible-light ultramicroscopy technique, Opt. Express 12 (7) (2004) 1214–1220.
[19] B.S. Luk'yanchuk, R. Paniagua-Domínguez, I. Minin, O. Minin, Z. Wang, Refractive index less than two: photonic nanojets yesterday, today and tomorrow, Opt. Mater. Express 7 (6) (2017) 1820–1847.
[20] Z. Wang, W. Guo, L. Li, B. Luk'Yanchuk, A. Khan, Z. Liu, Z. Chen, M. Hong, Optical virtual imaging at 50 nm lateral resolution with a white-light nanoscope, Nature Commun. 2 (1) (2011) 1–6.
[21] E. Mcleod, C.B. Arnold, Subwavelength direct-write nanopatterning using optically trapped microspheres, Nature Nanotechnol. 3 (7) (2008) 413–417.
[22] H. Yang, M. Cornaglia, M.A. Gijs, Photonic nanojet array for fast detection of single nanoparticles in a flow, Nano Lett. 15 (3) (2015) 1730–1735.
[23] I. Alessandri, N. Bontempi, L. Depero, Colloidal lenses as universal Raman scattering enhancers, RSC Adv. 4 (72) (2014) 38152–38158.
[24] Y. Li, X. Liu, B. Li, Single-cell biomagnifier for optical nanoscopes and nanotweezers, Light Sci. Appl. 8 (1) (2019) 1–12.
[25] Y. Li, H. Xin, X. Liu, Y. Zhang, H. Lei, B. Li, Trapping and detection of nanoparticles and cells using a parallel photonic nanojet array, ACS Nano 10 (6) (2016) 5800–5808.
[26] H. Wang, X. Wu, D. Shen, Trapping and manipulating nanoparticles in photonic nanojets, Opt. Lett. 41 (7) (2016) 1652–1655.
[27] X. Cui, D. Erni, C. Hafner, Optical forces on metallic nanoparticles induced by a photonic nanojet, Opt. Express 16 (18) (2008) 13560–13568.
[28] A.S. Ang, A. Karabchevsky, I.V. Minin, O.V. Minin, S.V. Sukhov, A.S. Shalin, 'Photonic hook'based optomechanical nanoparticle manipulator, Sci. Rep. 8 (1) (2018) 1–7.
[29] Y.E. Geints, O.V. Minin, L. Yue, I.V. Minin, Wavelength-scale photonic space switch proof-of-concept based on photonic hook effect, Ann. Phys. 533 (9) (2021) 2100192.
[30] V. Pacheco-Peña, J.A. Riley, C.-Y. Liu, O.V. Minin, I.V. Minin, Diffraction limited photonic hook via scattering and diffraction of dual-dielectric structures, Sci. Rep. 11 (1) (2021) 20278.
[31] C.-Y. Liu, H.-J. Chung, E. Hsuan-Pei, Reflective photonic hook achieved by a dielectric-coated concave hemicylindrical mirror, J. Opt. Soc. Amer. B 37 (9) (2020) 2528–2533.
[32] G. Gu, L. Shao, J. Song, J. Qu, K. Zheng, X. Shen, Z. Peng, J. Hu, X. Chen, M. Chen, et al., Photonic hooks from Janus microcylinders, Opt. Express 27 (26) (2019) 37771–37780.
[33] I.V. Minin, O.V. Minin, C.-Y. Liu, H.-D. Wei, Y.E. Geints, A. Karabchevsky, Experimental demonstration of a tunable photonic hook by a partially illuminated dielectric microcylinder, Opt. Lett. 45 (17) (2020) 4899–4902.
[34] T. Elbaz, A. Chauhan, A. Halstuch, G. Shalev, A. Karabchevsky, Step-index (semi-immersed) model for photonic nanojet and experimental characterization via near-field optical microscopy with microcylinder, Nanomaterials 13 (6) (2023) 1033.
[35] L. Yue, O.V. Minin, Z. Wang, J.N. Monks, A.S. Shalin, I.V. Minin, Photonic hook: a new curved light beam, Opt. Lett. 43 (4) (2018) 771–774.
[36] Y. Zhang, C.-W. Lo, J.A. Taylor, S. Yang, Replica molding of high-aspect-ratio polymeric nanopillar arrays with high fidelity, Langmuir 22 (20) (2006) 8595–8601.
[37] L. Novotny, B. Hecht, Principles of Nano-Optics, Cambridge University Press, 2012.
[38] I.V. Minin, O.V. Minin, Y. Cao, Z. Liu, Y.E. Geints, A. Karabchevsky, Optical vacuum cleaner by optomechanical manipulation of nanoparticles using nanostructured mesoscale dielectric cuboid, Sci. Rep. 9 (1) (2019) 1–8.
[39] K. Svoboda, S.M. Block, Optical trapping of metallic Rayleigh particles, Opt. Lett. 19 (13) (1994) 930–932.
[40] P.B. Johnson, R.-W. Christy, Optical constants of the noble metals, Phys. Rev. B 6 (12) (1972) 4370.
[41] M. Spector, A.S. Ang, O.V. Minin, I.V. Minin, A. Karabchevsky, Photonic hook formation in near-infrared with MXene Ti 3 C 2 nanoparticles, Nanoscale Adv. 2 (11) (2020) 5312–5318.